UNIVERSITÉ DE GENÈVE

Archive ouverte UNIGE
https://archive-ouverte.unige.ch

Article scientifique | Article | 2022

Accepted version | Open Access

This is an author manuscript post-peer-reviewing (accepted version) of the original publication. The layout of the published version may differ .

Quenching the bandgap of two-dimensional semiconductors with a perpendicular electric field

Domaretskiy, Daniil; Philippi, Marc; Gibertini, Marco; Ubrig, Nicolas; Gutierrez Lezama, Ignacio; Morpurgo, Alberto

How to cite

DOMARETSKIY, Daniil et al. Quenching the bandgap of two-dimensional semiconductors with a perpendicular electric field. In: Nature nanotechnology, 2022. doi: 10.1038/s41565-022-01183-4

This publication URL: https://archive-ouverte.unige.ch/unige:162807
Publication DOI: 10.1038/s41565-022-01183-4

© This document is protected by copyright. Please refer to copyright holder(s) for terms of use.

Quenching the band gap of 2D semiconductors with a perpendicular electric field

Daniil Domaretskiy,[1,2,*] Marc Philippi,[1,2,*] Marco Gibertini,[1,3,4] Nicolas Ubrig,[1,2] Ignacio Gutiérrez-Lezama,[1,2] and Alberto F. Morpurgo[1,2,†]

[1] *Department of Quantum Matter Physics, University of Geneva, 24 Quai Ernest Ansermet, CH-1211 Geneva, Switzerland*

[2] *Group of Applied Physics, University of Geneva, 24 Quai Ernest Ansermet, CH-1211 Geneva, Switzerland*

[3] *Dipartimento di Scienze Fisiche, Informatiche e Matematiche, University of Modena and Reggio Emilia, IT-41125 Modena, Italy*

[4] *Centro S3, CNR-Istituto Nanoscienze, IT-41125 Modena, Italy*

(Dated: August 18, 2022)

Perpendicular electric fields can tune the electronic band structure of atomically thin semiconductors. In bilayer graphene, which is an intrinsic zero-gap semiconductor, a perpendicular electric field opens a finite band gap. So far, however, the same principle could not be applied to control the properties of a broader class of 2D materials, because the required electric fields are beyond reach in current devices. To overcome this limitation, we design double ionic gated transistors that enable the application of large electric fields up to 3 V/nm. Using such devices, we continuously supress the band gap of few-layer semiconducting transition metal dichalcogenides, bilayer to heptalayer WSe_2, from 1.6 V to zero. Our results illustrate an unprecedented level of control on the band structure of 2D semiconductors.

An electric field applied perpendicular to the surface of a bulk semiconductor is screened over a finite length, leaving the material interior unaffected. In atomically thin semiconductors [1], however, the small thickness prevents efficient screening, so that a perpendicular electric field uniformly influences the entire system, modifying its band structure [2–11]. Indeed, a zero-gap semiconductor such as bilayer graphene can be turned into a gapped insulator using double-gated transistors to apply a perpendicular electric field [2–4]. Despite representing a breakthrough, continuous control of the band structure in transistors has not found widespread use because –as it has become apparent in multiple, recent experiments [7, 10, 12]– the limited maximum electric field that can be applied in common devices does not allow significant changes to be induced in most 2D materials. Indeed, whereas theory [5, 9], and our own calculations (see Supplementary Note S8), predict that sufficiently strong fields can quench the band gap of few layer semiconductors, earlier works [7, 12] have only shown a 10 % gap reduction (or less) at fields reached in conventional double-gated transistors.

Electric fields sufficient to quench the gap of atomically thin semiconductors can be achieved in ionic gate transistors. Owing to the huge capacitance of electrolytes (≈

* These authors have contributed equally

† alberto.morpurgo@unige.ch

$50\mu F/cm^2$ [13–18]), ionic gated devices [14–16, 19] can accumulate charge densities unattainable with conventional gating that enable the observation of new physical phenomena [14, 15, 20–25]. Associated to the high densities are extremely large electric fields, which in a double gate geometry could be controlled independently from the accumulated charge, by applying opposite voltages to the top and back gates. So far, however, the technical complexity has prevented the realization of double ionic gated devices. Here, we demonstrate double ionic gate transistors that allow the application of electric fields up to 3 V/nm, and use them to fully quench band gaps as large as 1.6 eV in WSe_2 bilayers and thicker multilayers.

Double ionic gate transistors for large electric fields

In our devices (see Methods and Supplementary Note S1 for details on device fabrication), two electrolytes in contact with two independent gate electrodes are coupled to the same atomically thin semiconductor (see Fig. 1**a**). The top electrolyte is a commonly used ionic liquid ($[P14]^+$-$[FAP]^-$) [14–16, 18, 19, 26, 27], and the bottom one is a Li-ion glass ceramic substrate [17, 28] (LASPT[29]). The atomically thin semiconductor is connected to two metal source and drain electrodes, and surrounded by a ground plane (an Aluminum film sandwiched between two Al_2O_3 layers). The ground plane leaves exposed to the ionic liquid only the 2D semiconductor and eliminates any direct electrostatic coupling of the top and bottom electrolyte. This is important: if the two electrolytes were in direct contact, they would equilibrate their potential (as it happens in recently realized double-side ionic gated devices [30], with a single ionic liquid in contact with opposite surfaces of a 2D semiconductor), preventing the potential of the bottom and of the top electrolyte to be controlled independently. A perpendicular electric field with no net charge accumulation is established across atomically thin multilayers by applying a positive voltage V_{IL} to the ionic liquid gate and a negative voltage V_{BG} to the back gate. Because of the very large capacitance of both electrolytes, most of the applied potential difference drops across the gated material, enabling electric fields in excess of 3 V/nm to be reached (see Supplementary Note S5 for a detailed analysis).

Quenching the band gap of 2D semiconductors

In single ionic-gate devices, conductivity measurements as a function of gate voltage

provide spectroscopic capabilities, enabling band gaps of individual 2D semiconductors to be determined quantitatively [19]. In double gated devices, we apply the same technique to determine the presence or absence of a gap. In simple terms, gate-induced transport can be mediated by electrons –when a positive gate voltage sets the chemical potential in the conduction band– or by holes –when a negative applied gate voltage sets the chemical potential in the valence band. The two regimes are separated by a gate voltage interval in which transport is strongly suppressed, with the chemical potential located in the gap. To determine whether the gap can be quenched, we look at the interval of gate voltages over which transport is suppressed, and see whether its extension can be reduced to zero by applying a perpendicular electric field. To this end, we measure the gate-induced device conductivity as a function of V_{IL} and V_{BG}, and plot it versus $V^\star = V_{IL} + V_{BG}$ (proportional to the potential applied to the semiconductor channel), for different values of $E^\star = V_{IL} - V_{BG}$ (proportional to the applied electric field, see Supplementary Note S5). Before discussing data plotted in this way it is however useful to analyze different aspects of the device behavior.

When one gate voltage is swept keeping the other gate grounded, double gate devices function as conventional transistors, as illustrated by the transfer curves (I_{SD} as a function of gate voltage) recorded on a WSe_2 bilayer (2L) device (see Fig. 1**b** and 1**c**, measured with $V_{IL} =$ 0 V and $V_{BG} =$ 0 V, respectively; for additional characterization measurements, see Supplementary Note S2). These curves are virtually identical to those measured on single gated devices, but for increasing negative V_{BG} values (Fig. 2**a**) the transfer curves I_{SD}-vs-V_{IL} evolve. For V_{BG} = - 0.4 V, the transfer curve is still similar to that measured for V_{BG} = 0 V (Fig. 1**c**): the current I_{SD} increases as V_{IL} is swept past the threshold for electron accumulation (V_{IL} = 1.8 V), and no current flows for $V_{IL} < 1.8$ V, when the chemical potential is in the gap. At $V_{BG} \sim$ -1 V, however, the transfer curve exhibits qualitative differences, as current flows even for V_{IL} well below 1.8 V. As V_{BG} is set to more negative values, the source-drain current I_{SD} remains large for all values of V_{IL}, without ever vanishing (the square resistance $R_{sq} \sim h/e^2$ for all V_{IL}). Analogous considerations hold true when looking at the evolution of the I_{SD}-vs-V_{BG} curve upon applying a positive voltage V_{IL} to the ionic liquid gate (Fig 2**b**).

The color plot in Fig. 2**c** shows the complete evolution of I_{SD} as a function of V_{IL} and

V_{BG}. The measurements are fully reproducible and reversible, as discussed in Supplementary Note S4. The observed behavior is not the one expected if the only effect of the gate voltages was to affect the electrostatic potential in the transistor channel, i.e., the mechanism that determines the operation of a conventional transistor. In that case, both V_{IL} and V_{BG} would just shift the energy of the 2L-WSe_2 bands, and a change in the voltage applied to one gate would only cause a rigid shift in the transfer curve measured as a function of the voltage applied to the other. The data, however, do not show a rigid shift. The observed behavior is also not the one expected in devices in which the two gates are decoupled [31], i.e., in which transport would be mediated by two accumulation layers of electrons and holes on opposite surfaces of the bilayer (see Supplementary Note S6 and Supplementary Fig. S10).

The reason is that the concomitant application of large positive V_{IL} and large negative V_{BG} generates a perpendicular electric field that quenches the band gap. To gain further understanding, we look at the evolution of transport as V_{IL} and V_{BG} are varied continuously along the contour outlined by the colored line in Fig. 2**c**. At point A, V_{IL} = 0 V and V_{BG} = -2.4 V. The negative potential V_{BG} results in the accumulation of holes (see Fig. 1**b**), and sets the chemical potential in the WSe_2 valence band. As V_{IL} is increased from 0 to 2.4 V at fixed V_{BG} = -2.4 V, we travel from points A to B (green line), and the electrostatic potential $V^\star$ applied to the channel vanishes. Nevertheless, the current remains large. If then V_{BG} is decreased from -2.4 to 0 V at fixed V_{IL} = 2.4 V we move from B to C (purple line), where transport is mediated by electrons accumulated by the large positive voltage V_{IL} (see Fig. 1**c**). Transport therefore evolves from being mediated by holes at point A (with the chemical potential in the valence band), to being mediated by electrons at point C (with the chemical potential in the conduction band), without ever passing through a highly insulating state (see Fig. 2**d**). This is possible only if the gap closes and the conduction and valence band overlap in some part of the contour, with electrons and holes coexisting in the transistor channel. Indeed, this happens in the neighborhood of B, where the electric field perpendicular to the 2L-WSe_2–proportional to $E^\star$– is maximum.

We now plot the current I_{SD} as a function of $V^\star = V_{IL}+V_{BG}$ and $E^\star = V_{IL}$ - V_{BG} (Fig. 3**a**). Fig. 3**b** shows I_{SD}-vs-$V^\star$ curves measured at fixed values of $E^\star$. As expected, at small $E^\star$, I_{SD} is finite for sufficiently large negative and positive $V^\star$ –with current carried

by holes and electrons– and vanishes over an extended $V^\star$ interval, as the chemical potential is swept across the 2L-WSe_2 gap (the square resistance in this regime is larger than the our measurement sensitivity). The $V^\star$ interval with vanishing current shrinks as $E^\star$ increases and for $E^\star > E_c^\star$, no highly resistive state is observed. This signals a transition to a highly conductive state with increasing applied perpendicular electric field, which becomes apparent by looking at the evolution of I_{SD}-vs-$E^\star$ at fixed values of $V^\star$, i.e., by looking at vertical cuts of the color plot shown in Fig. 3**a**. In Fig. 3**c** we plot such a cut for $V^\star = 0.5$ V (dashed green line in Fig. 3**a**), showing that for sufficiently large values of $E^\star$ (> 3V) I_{SD} increases with increasing $E^\star$ without a change in the electrostatic potential applied to the channel. We conclude that in the presence of a sufficiently large electric field a finite conductivity of order e^2/h is present irrespective of the position of the Fermi level, indicating that states are available at all energies to mediate transport. This implies that no gap is present and that the application of a sufficiently large electric field fully quenches the 2L-WSe_2 band gap.

To determine $E_c^\star$, we extract the electron and hole threshold voltages ($V_{T-e}^\star$ and $V_{T-h}^\star$), plot their difference $\delta = V_{T-e}^\star - V_{T-h}^\star$ as a function of $E^\star$, and look at when δ vanishes (Fig. 3**d**). The corresponding electric field is then approximately given by $E_c^\star/t_{TMD} \simeq 3.0$ V/nm, where $t_{TMD} = 1.3$ nm is the 2L-WSe_2 thickness. This is a good approximation because of the very large gate capacitance ($C \approx 50\ \mu F/cm^2$ [13, 14, 16–18]), which ensures that the voltage drop across the electrolytes is small (see discussion in Supplementary Note S5). We conclude that the electric field $\mathscr{E}_c$ needed to quench the 2L WSe_2 gap is between 2.5 and 2.7 V/nm (this is the electric field, not the displacement field, frequently quoted when analyzing experiments on double-gated transistors in the literature). We have performed similar experiments on 3L, 4L, 5L and 7L WSe_2 and succeeded in closing the band gap in all cases (see Fig. 4 for data measured on devices of different thickness). For some of these devices we have also looked at the evolution of the I_{SD}-vs-V_{SD} curves upon increasing perpendicular electric field, and observed a behavior confirming that the gap actually closes (see Supplementary Note S7 and Supplementary Fig. S11).

The critical electric field $\mathscr{E}_c$ required to close the gap –crosses in Fig. 4**g**– decreases upon increasing thickness. It quantitatively matches theoretical predictions based on ab-initio calculations, validating the interpretation of our experiments. Earlier studies [32, 33] have

reported a metallic state originating from a structural transition of $MoTe_2$ from the 2H structure to the so-called 1T' structure, resulting from either gate-induced charge accumulation [32] or from the application of an electric field [33]. In both cases, the structural transition was accompanied by a very large hysteresis: upon reducing the accumulated charge density or the applied electric field, the system remained in the highly conducting state (structural transitions of the type invoked are typically of first order). This is not what is seen in our data: neither a discontinuous transition nor any sizable hysteresis in conductivity is observed in the measurements (see Supplementary Note 4). We can therefore exclude a structural effect as the origin of the observed gap quenching.

Gap quenching versus decoupled accumulation layers

The experimental results show that in the presence of a sufficiently large perpendicular electric field, the atomically thin WSe_2 multilayers that we have investigated remain conducting, irrespective of the position of the chemical potential, with a minimum conductivity of order e^2/h. This observation directly indicates that at sufficiently large applied electric field a finite density of states is present at all energies, i.e. the gap closes. Because the multilayers are only a few atom thick, a fully quantum mechanical calculation is needed to understand how the gap closes. In simple qualitative terms, however, a sufficiently large perpendicular electric field quenches the gap because the electrostatic potential lifts the energy of the valence band edge at one crystal surface above the conduction band edge at the opposite surface. The conduction and valence bands then overlap, and the system becomes gapless.

One may then wonder whether the closing of the gap and the gate dependence of the conductivity that we observe is not simply due to the formation of two decoupled accumulation layers –one of electrons and one of holes– at the opposite multilayer surfaces, as is happens in macroscopically thick crystals [31]. However, neither modeling the gate dependence in terms of decoupled accumulation layers, nor the experimental data measured on a 70 nm thick double-ionic gated WSe_2 crystal, reproduce key aspects of the dependence of I_{SD} on V_{IL} and V_{BG} observed on our atomically thin devices (see Supplementary Note S6 and Fig. S10). That is because, for atomically thin multilayers (certainly for 2L and 3L WSe_2), the extension of the electron and hole wavefunction is larger than the multilayer thickness, so

that the two surfaces overlap in real space. The extension of the wavefunction is governed by the electrostatic screening length that near charge neutrality (when the two gate voltages are equal and opposite) is longer than the multilayer thickness, because the electron and hole density is small (in double gated devices for fields $\mathscr{E}$ close to $\mathscr{E}_c$ the perpendicular electric field is large and the carrier density small, because field and density are controlled independently; such a regime of large field and small density cannot occur in single gated devices, in which a large electric field is necessarily accompanied by a large charge density). In these atomically thin multilayers, therefore, the electric field is large enough to bring spatially overlapping conduction and valence band states to the same energy, causing a drastic modification of the multilayer band structure. This is indeed what is predicted by *ab-initio* calculations (compare Fig. 1**d** and Fig. 1**e**), which show that at large electric field the gap closes as the minimum of the conduction band at the Q-point in the Brillouin zone touches the top of the valence band at the K-point (see Fig. 1**e**). We have extracted from these calculations the full thickness dependence of the critical electric field $\mathscr{E}_c$ needed to quench the gap and found excellent quantitative agreement with the values of $\mathscr{E}_c$ measured experimentally (see Fig. 4**h**). This agreement provides strong support for our interpretation.

Nature of the gapless state

The discussion above provides a basic physical scenario for the nature of the gapless electronic state of atomically thin WSe_2 multilayers. At charge neutrality, for applied electric fields $\mathscr{E} > \mathscr{E}_c$, these systems are compensated semimetals with a finite band overlap that increases with increasing $\mathscr{E}$, with coexisting electron and hole states. The semimetal has broken inversion symmetry, owing to the large electric field present. It is uniform in the plane of the multilayer, but the "center of mass" of electrons and holes are displaced relative to each other in the direction perpendicular to the layers. As the electric field is increased, the electron and hole states are pushed away from each other due both to the increasing potential difference between the two surfaces and to the fact that –as the electron and hole densities increase– the screening length may eventually become shorter than the thickness. At that point, the system will effectively consist of electron and hole accumulation layers that are coupled only by Coulomb attraction. For the thinnest multilayers, such as 2L and 3L WSe_2, however, the thickness is so small that full overlap of the electron and hole wavefunctions remains relevant even at the largest experimentally accessible densities. An

investigation of transport and of the optical response as a function of perpendicular electric field and temperature will clearly be essential to understand the properties of atomically thin WSe_2 multilayers with an electrically tunable band gap.

Conclusion

We have established the ability to quench a semiconducting band gap larger than 1.6 eV in 2D semiconductors as thin as a WSe_2 bilayer (i.e., just over 1 nm thick), by applying a very large perpendicular electric field, close to 3 V/nm. The ability to control the semiconducting gap and to reversibly apply electric fields of 3 V/nm onto a 2D material have great potential for future studies. Indeed, many theoretical studies have been reported, predicting that the electronic properties of a variety of atomically thin crystals can be drastically altered if fields of this strength can be reached in the experiments. Examples include topological transitions in transition metal dichalcogenides [34–36] and other 2D materials [37], the ability to switch the magnetic anisotropy [38] or the topological charge of magnetic excitations [39], and the control of the electronic state and other properties of different van der Waals materials and of their heterostructures [40–42]. So far, these theoretical predictions were considered to be exclusively of academic interest, because the required electric fields were nearly one order of magnitude larger than those reachable in practice. The results shown here change the situation, as they allow a vast gamut of unexplored electronic phenomena to be investigated experimentally.

Note added at submission At the time of submission we became aware of a manuscript by B. I. Weintrub *et al.* that has just appeared on the Cond-mat public archive [43] and that reports experiments similar to the ones discussed here.

ACKNOWLEDGEMENTS

The authors thank A. Ferreira for technical support. A.F.M. acknowledges financial support from the Swiss National Science Foundation (Division II) and from the EU Graphene Flagship project. M.G. acknowledges support from the Italian Ministry for University and Research through the Levi-Montalcini program.

AUTHOR CONTRIBUTIONS

D.D., M.P., N.U., and I.G.L. fabricated the devices and carried out the experiments. D.D, M.P., I.G.L, and A.F.M. analysed the experimental data. M.G. performed first-principles simulations. I.G.L. supervised the experimental work and A.F.M. conceived and directed the research. All authors participated in preparing the manuscript.

COMPETING INTERESTS

The authors declare no competing interests.

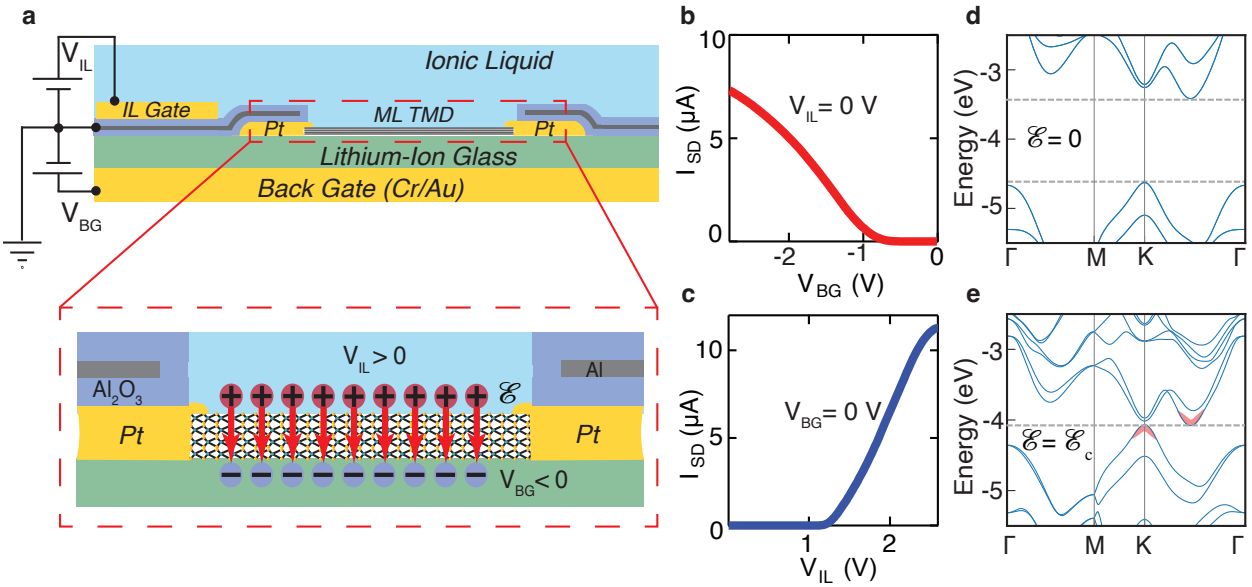

FIG. 1. **Double ionic gated field-effect transistors.** **a** (top panel) Schematic cross-section of a multilayer WSe_2 transistor equipped with a top ionic liquid (IL) gate and Li-ion conductive glass ceramic back gate (BG). Also shown are the Pt contacts to the TMD multilayer and a $Al_2O_3/Al/Al_2O_3$ trilayer to decouple electrostatically the top and bottom electrolytes. (bottom panel) Zoom in on the device channel area (not to scale). When the two gates are biased with opposite polarity the charges accumulated on the double layers of the two electrolytes (schematically shown in the figure as red and blue balls) compensate, and a uniform perpendicular electric field $\mathscr{E}$ is established across the TMD (represented by the red arrows in the scheme). **b** Source-drain current I_{SD} measured on a WSe_2 bilayer device, for negative back gate voltages V_{BG} applied to the Li-ion glass gate (with the ionic liquid gate grounded, V_{IL}= 0 V), resulting in the accumulation of holes. **c** I_{SD} measured on the same device as a function of $V_{IL} > 0$ V for $V_{BG} = 0$ V, to cause electron accumulation (the applied source-drain voltage is $V_{SD} = 0.1$ V in **b** and **c**). Note that the application of positive V_{IL} and negative $V_{BG} < 0$ V causes the Li ions to be pulled away from the TMD, ensuring that intercalation does not take place. **d** and **e** represent the band structure of 2L WSe_2 computed within density-functional theory –respectively for zero perpendicular electric $\mathscr{E} = 0$ V/nm, and at the critical field $\mathscr{E} = \mathscr{E}_c$– and show that quenching of the gap with an electric field is expected theoretically (see Supplementary Note S8 for details; in (**e**), the conduction and valence band edge at $\mathscr{E}_c$ are denoted by red shaded lines). Γ, M and K are high symmetry points along the Brillouin zone of the hexagonal lattice of WSe_2.

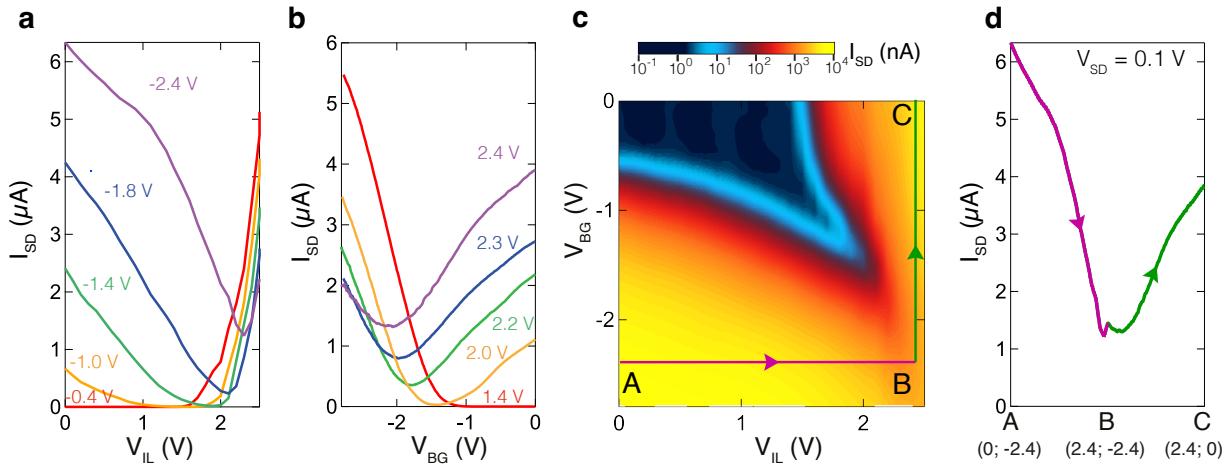

FIG. 2. **Electrical characteristics of a double-gated 2L-WSe_2 transistor.** **a** Source-drain current I_{SD} measured on a 2L-WSe_2 device as a function of ionic liquid gate voltage V_{IL}, for different negative values of back gate voltage V_{BG}. The curves evolve from exhibiting textbook transistor behavior at small negative V_{BG} (see also Fig. 1**b**), to not showing any sizable current suppression at large negative V_{BG}. **b** Same as **a**, with the source-drain current I_{SD} measured as a function of V_{BG} for different positive values of V_{IL}; the evolution of the transistor curves is fully analogous to the one shown in **a**. **c** Color plot of I_{SD} (in logarithmic scale) as a function of V_{BG} and V_{IL}. Note that the simultaneous application of a large negative V_{BG} and of an equally large positive V_{IL} causes the current in the transistor to increase by 4-to-5 orders of magnitude, despite leaving the potential of the transistor channel ($V^\star = V_{IL} + V_{BG}$) unchanged. **d** Evolution of I_{SD} along the A-B-C contour illustrated in panel (**d**) (the coordinates of A, B, and C in the (V_{IL}, V_{BG}) plane are indicated at the bottom). Transport in the transistor is mediated by holes at A and by electrons at C: finding that nowhere the current is fully suppressed implies that on part of the A-B-C contour the valence and conduction band of WSe_2 must overlap. In all measurements the applied source-drain voltage is $V_{SD} = 0.1$ V.

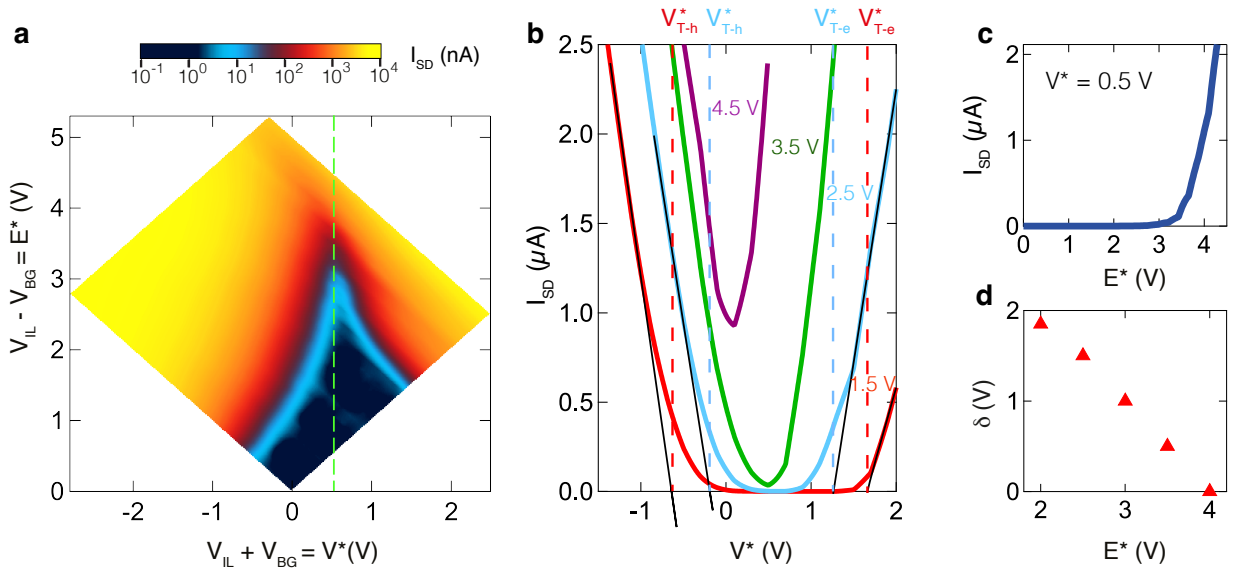

FIG. 3. **Band gap evolution as a function of electric field.** **a** Colour plot of the source-drain current I_{SD} (in logarithmic scale) measured on a WSe_2 bilayer device as a function of $V^\star = V_{IL} + V_{BG}$, and $E^\star = V_{IL} - V_{BG}$ (respectively proportional to the electrostatic potential in the transistor channel and to the electric field perpendicular to the 2L-WSe_2 crystal). The width of the $V^\star$ interval over which the current I_{SD} is suppressed decreases monotonically upon increasing $E^\star$. **b** For a quantitative analysis, we look at horizontal cuts of the color plot in (**a**), I_{SD}-vs-$V^\star$ at fixed $E^\star$ (values indicated in the figure). The curve measured at $E^\star = 4.5$ V exhibits a complete suppression of I_{SD}, and the black thin lines illustrate how we determine the threshold voltage for electron ($V^\star_{T-e}$) and hole ($V^\star_{T-h}$) conduction (by extrapolating I_{SD} to zero for positive and negative values of $V^\star$; the position of the threshold voltages are marked by the vertical dashed lines). **c** Cut of the color plot in **a**, taken at fixed $V^\star = 0.5$ V, in correspondence of the vertical green dashed line. The data show a transition from a highly resistive state at low $E^\star$, to a state with conductivity of order h/e^2 at $E^\star > 4$ V. This transition, which occurs at fixed V^*, is a direct manifestation of the quenching of the band gap caused by the applied electric field. **d** We plot $\delta = V^\star_{T-e} - V^\star_{T-h}$ as a function of $E^\star$, and find the value $E^\star_c$ for which $\delta = 0$ V ($E^\star_c = 4$ V in our 2L-WSe_2 device) to determine the condition at which the gap closes.

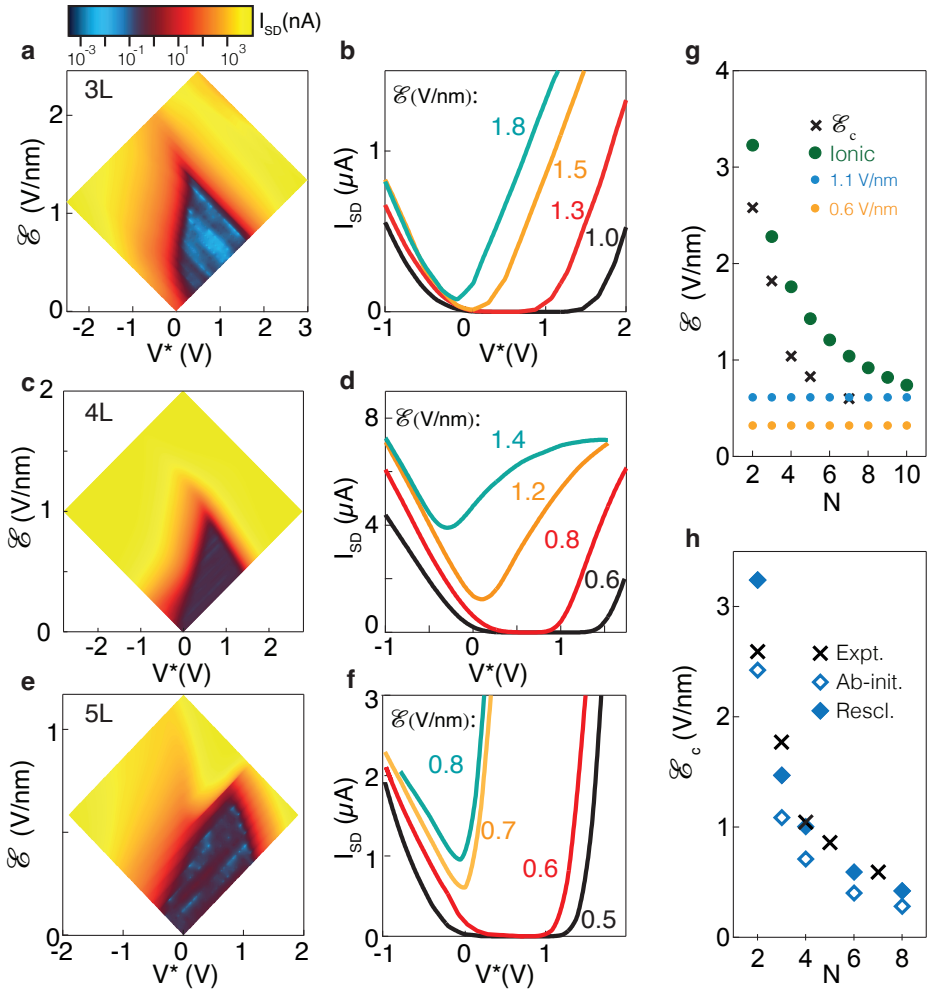

FIG. 4. **Quenching the gap in 3L, 4L and 5L WSe_2 devices**. **a**,**c** and **e** show color plots of the source-drain current I_{SD} as a function of $V^\star = V_{IL} + V_{BG}$ (sum of ionic liquid and back gate voltages) and the electric field $\mathscr{E}$ for 3L, 4L, and 5L devices. **b**,**d**,**f** show the corresponding cuts (I_{SD}-vs-V^*), for different fixed values of electric field $\mathscr{E}$ across each WSe_2 multilayer. **g** Comparison between the maximum electric fields that can be applied across WSe_2 N-layers, using different type of devices. Green dots: field achieved in ionic gated devices for $E^\star = V_{IL} - V_{BG} = 5$ V (larger values are possible, as we repeatedly reached 5.5 and 6 V; see Supplementary Note S5 for details on the estimation of $\mathscr{E}$); blue and orange dots: maximum field reachable with hBN-based devices assuming a breakdown field of 1.1 V/nm and 0.6 V/nm, respectively (1.1 V/nm is the ultimate limit reached in ultra-thin hBN; 0.6 V/nm is a more realistic estimate for common hBN). For bilayer WSe_2, the electric field reachable with ionic gating is nearly one order of magnitude larger than the field accessible in hBN-based devices. The dark crosses are the field needed to close the gap, as extracted from our measurements: for all thicknesses it would have not been possible to close the gap with hBN-based devices. **h** Comparison between the critical electric fields $\mathscr{E}_c$ extracted from experiments (dark crosses) and the corresponding theoretical values obtained from first principle calculations (empty diamonds). *Ab-initio* calculations slightly underestimate the gap, resulting in a small underestimate of $\mathscr{E}_c$. To take this into account, the full diamonds show the value of the critical electric field obtained using the ratio between the known and the calculated gap to rescale $\mathscr{E}_c$ (see Supplementary Note S8). The agreement with experiments is excellent.

[1] Novoselov, K. S. *et al.* Two-dimensional atomic crystals. *PNAS* **102**, 10451–10453 (2005).

[2] Oostinga, J. B., Heersche, H. B., Liu, X., Morpurgo, A. F. & Vandersypen, L. M. K. Gate-induced insulating state in bilayer graphene devices. *Nature Materials* **7**, 151–157 (2008).

[3] Zhang, Y. *et al.* Direct observation of a widely tunable bandgap in bilayer graphene. *Nature* **459**, 820–823 (2009).

[4] Mak, K. F., Lui, C. H., Shan, J. & Heinz, T. F. Observation of an Electric-Field-Induced Band Gap in Bilayer Graphene by Infrared Spectroscopy. *Phys. Rev. Lett.* **102**, 256405 (2009).

[5] Ramasubramaniam, A., Naveh, D. & Towe, E. Tunable band gaps in bilayer transition-metal dichalcogenides. *Physical Review B* **84**, 205325 (2011).

[6] Drummond, N. D., Zólyomi, V. & Fal'ko, V. I. Electrically tunable band gap in silicene. *Physical Review B* **85**, 075423 (2012).

[7] Chu, T., Ilatikhameneh, H., Klimeck, G., Rahman, R. & Chen, Z. Electrically Tunable Bandgaps in Bilayer MoS_2. *Nano Letters* **15**, 8000–8007 (2015).

[8] Kim, J. *et al.* Observation of tunable band gap and anisotropic Dirac semimetal state in black phosphorus. *Science* **349**, 723–726 (2015).

[9] Dai, X., Li, W., Wang, T., Wang, X. & Zhai, C. Bandstructure modulation of two-dimensional WSe_2 by electric field. *Journal of Applied Physics* **117**, 084310 (2015).

[10] Deng, B. *et al.* Efficient electrical control of thin-film black phosphorus bandgap. *Nature Communications* **8**, 14474 (2017).

[11] Overweg, H. *et al.* Electrostatically Induced Quantum Point Contacts in Bilayer Graphene. *Nano Letters* **18**, 553–559 (2018).

[12] Chen, P. *et al.* Band evolution of two-dimensional transition metal dichalcogenides under electric fields. *Appl. Phys. Lett.* **115**, 083104 (2019). Publisher: American Institute of Physics.

[13] Yuan, H. *et al.* High-Density Carrier Accumulation in ZnO Field-Effect Transistors Gated by Electric Double Layers of Ionic Liquids. *Advanced Functional Materials* **19**, 1046–1053 (2009).

[14] Fujimoto, T. & Awaga, K. Electric-double-layer field-effect transistors with ionic liquids. *Physical Chemistry Chemical Physics* **15**, 8983–9006 (2013).

[15] Bisri, S. Z., Shimizu, S., Nakano, M. & Iwasa, Y. Endeavor of Iontronics: From Fundamentals to Applications of Ion-Controlled Electronics. *Advanced Materials* **29**, 1607054 (2017).

[16] Schmidt, E., Shi, S., Ruden, P. P. & Frisbie, C. D. Characterization of the Electric Double Layer Formation Dynamics of a Metal/Ionic Liquid/Metal Structure. *ACS Appl. Mater. Interfaces* **8**, 14879–14884 (2016).

[17] Philippi, M., Gutiérrez-Lezama, I., Ubrig, N. & Morpurgo, A. F. Lithium-ion conducting glass ceramics for electrostatic gating. *Applied Physics Letters* **113**, 033502 (2018).

[18] Zhang, H., Berthod, C., Berger, H., Giamarchi, T. & Morpurgo, A. F. Band Filling and Cross Quantum Capacitance in Ion-Gated Semiconducting Transition Metal Dichalcogenide Monolayers. *Nano Letters* **19**, 8836–8845 (2019).

[19] Gutiérrez-Lezama, I., Ubrig, N., Ponomarev, E. & Morpurgo, A. F. Ionic gate spectroscopy of 2D semiconductors. *Nature Reviews Physics* **3**, 1–12 (2021).

[20] Yamada, Y. *et al.* Electrically induced ferromagnetism at room temperature in cobalt-doped titanium dioxide. *Science* **332**, 1065–1067 (2011).

[21] Ye, J. T. *et al.* Superconducting Dome in a Gate-Tuned Band Insulator. *Science* **338**, 1193–1196 (2012).

[22] Wang, S., Ha, M., Manno, M., Daniel Frisbie, C. & Leighton, C. Hopping transport and the Hall effect near the insulator–metal transition in electrochemically gated poly(3-hexylthiophene) transistors. *Nature Communications* **3**, 1210 (2012).

[23] Lu, J. M. *et al.* Evidence for two-dimensional Ising superconductivity in gated MoS_2. *Science* **350** (2015).

[24] Costanzo, D., Jo, S., Berger, H. & Morpurgo, A. F. Gate-induced superconductivity in atomically thin MoS_2 crystals. *Nature Nanotechnology* **11**, 339–344 (2016).

[25] Leighton, C. Electrolyte-based ionic control of functional oxides. *Nature Materials* **18**, 13–18 (2019).

[26] Ponomarev, E., Ubrig, N., Gutiérrez-Lezama, I., Berger, H. & Morpurgo, A. F. Semiconducting van der waals interfaces as artificial semiconductors. *Nano Letters* **18**, 5146–5152 (2018).

[27] Reddy, B. A. *et al.* Synthetic semimetals with van der waals interfaces. *Nano Letters* **20**, 1322–1328 (2020).

[28] Alam, M. H. *et al.* Lithium-ion electrolytic substrates for sub-1V high-performance transition metal dichalcogenide transistors and amplifiers. *Nature Communications* **11**, 3203 (2020).

[29] Nakajima, K., Katoh, T., Inda, Y. & Hoffman, B. Lithium Ion Conductive Glass Ceramics: Properties and Application in Lithium Metal Batteries 28 (2010). URL http://oharacorp.com/pdf/ohara-presentation-ornl-symposium-10-08-2010.pdf.

[30] Zheliuk, O. *et al.* Josephson coupled Ising pairing induced in suspended MoS_2 bilayers by double-side ionic gating. *Nat. Nanotechnol.* **14**, 1123–1128 (2019).

[31] Ji, H. *et al.* Thickness effect on low-power driving of MoS_2 transistors in balanced double-gate fields. *Nanotechnology* **31**, 255201 (2020).

[32] Wang, Y. *et al.* Structural phase transition in monolayer $MoTe_2$ driven by electrostatic doping. *Nature* **550**, 487–491 (2017).

[33] Zhang, F. *et al.* Electric-field induced structural transition in vertical $MoTe_2$- and $Mo_{1-x}W_xTe_2$-based resistive memories. *Nature Materials* **18**, 55–61 (2019).

[34] Qian, X., Liu, J., Fu, L. & Li, J. Quantum spin Hall effect in two-dimensional transition metal dichalcogenides. *Science* **346**, 1344–1347 (2014).

[35] Tong, Q. *et al.* Topological mosaics in moiré superlattices of van der Waals heterobilayers. *Nature Physics* **13**, 356–362 (2017).

[36] Zhu, Q., Tu, M. W.-Y., Tong, Q. & Yao, W. Gate tuning from exciton superfluid to quantum anomalous Hall in van der Waals heterobilayer. *Science Advances* **5**, eaau6120 (2019).

[37] Marrazzo, A., Gibertini, M., Campi, D., Mounet, N. & Marzari, N. Prediction of a large-gap and switchable Kane-Mele quantum spin Hall insulator. *Phys. Rev. Lett.* **120**, 117701 (2018).

[38] Kim, D., Lee, C., Jang, B. G., Kim, K. & Shim, J. H. Drastic change of magnetic anisotropy in Fe_3GeTe_2 and Fe_4GeTe_2 monolayers under electric field studied by density functional theory. *Scientific Reports* **11**, 17567 (2021).

[39] Xu, C. *et al.* Electric-field switching of magnetic topological charge in type-I multiferroics. *Phys. Rev. Lett.* **125**, 037203 (2020).

[40] Wang, S. *et al.* Tunable Schottky barrier in graphene/graphene-like germanium carbide van der Waals heterostructure. *Scientific Reports* **9**, 5208 (2019).

[41] Wang, J. *et al.* Electric field-tunable structural phase transitions in monolayer tellurium. *ACS Omega* **5**, 18213–18217 (2020).

[42] Ke, C. *et al.* Tuning the electronic, optical, and magnetic properties of monolayer GaSe with a vertical electric field. *Phys. Rev. Applied* **9**, 044029 (2018).

[43] Weintrub, B. I., Hsieh, Y.-L., Kirchhof, J. N. & Bolotin, K. I. Dual ionic gate transistor: a device to induce extreme electric fields in 2d materials. *arXiv:2108.05797* (2020).

METHODS

Device fabrication

The double ionic gate transistors employed in our experiments use two electrostaticaly decoupled electrolytes to apply large perpendicular electric fields across atomically thin WSe_2 crystals. The top gate consists of a commonly used ionic liquid, 1-butyl-1-methylpyrrolidinium tris(pentafluorethyl)trifluorophosphate ($[P14]^+$-$[FAP]^-$; purchased from Merck Millipore, now VWR) coupled to a Pt/Au electrode, and the bottom gate consists of a Li-ion conductive glass ceramic (LASPT; purchased from MTI Corp) coupled to a Cr/Au electrode. The atomically thin WSe_2 crystals, ranging from 2 to 7 layers (and the 70 nm bulk-like crystal) were isolated via micro-mechanical cleavage of bulk crystals (purchased from HQ Graphene) onto SiO_2/Si substrates, and then transferred onto the Li-ion conductive glass ceramic using a common dry pick-up and transfer technique [1]. As described in Supplementary Note S1, atomically thin crystals can be identified optically on the glass ceramic [2], but it is preferable to transfer them form the SiO_2/Si substrates to avoid compromising the integrity of the Al_2O_3/Al/Al_2O_3 trilayer that decouples the two electrolytes. The electrical contacts to the crystals, the gate and reference (see below) electrodes are define by means of electron-beam lithography, electron-beam evaporation and lift-off or evaporation through a shadow mask (see Supplementary Note S1 for complete details on the electrode deposition).

To isolate and electrostatically decouple the Li-ion glass ceramic from the ionic liquid we employ an Al ground plane embedded between two Al_2O_3 layers (see Supplementary Note S1 for details on the deposition of the Al_2O_3/Al/Al_2O_3 trilayer). The presence of the ground plane is crucial for correct device operation, as without it the two electrolytes would equilibrate their potential and the the two gates could not longer be controlled independently. The effectiveness of the electrostatic decoupling can be checked experimentally using two

reference electrodes in direct contact with either the Li-ion glass or the top ionic liquid, as discussed in detail in Supplementary Note S3. The $Al_2O_3/Al/Al_2O_3$ trilayer also prevents diffusion of Li-ion from the substrate into the ionic liquid that causes degradation of the ionic liquid itself.

Transport measurements

All the electrical measurements performed during this work were carried out at room temperature and under high vacuum (1 x 10^{-6} mbar), using home-built voltage and current amplifiers in conjunction with DC source-measuring units (Keithley K2400) and digital multimeters (Agilent 3410).

In the double gated experiments all the measurements are done by applying a positive voltage to the ionic liquid and a negative voltage to the back gate, since under these conditions Li ions in the glass substrate are pushed away from the semiconducting layer, and cannot intercalate. Under this condition the measurements are fully reversible and reproducible. If the gate voltages are swept sufficiently slowly –the typical sweeping rate in our measurements is 5 mV/s– the measurements exhibit negligible or at most small hysteresis originating from bias stress effects (see Supplementary Note S4). In different measurements, the applied source drain bias was varied between 10 and 100 mV, to keep it smaller or comparable than the thermal energy $\simeq 3.5\ k_BT/e$, without any qualitative influence on the measurements.

First-principle simulations

In order to compute the critical electric field $\mathscr{E}_c$ at which the energy gap of a WSe_2 multilayer vanishes, we have carried out first-principles density-functional-theory (DFT) simulations within the Perdew-Burke-Ernzerhof (PBE) [3] generalized-gradient approximation as implemented in the Quantum ESPRESSO distribution [4, 5]. Here we outline the main technical aspects of our calculations and present the results.

In our calculations, the crystal structure of multilayers is obtained from the experimentally reported structure of bulk WSe_2, by cutting out a certain number of layers, without further relaxations. The Brillouin zone is sampled with $12 \times 12 \times 1$ k-points in a uniform Γ-

centered Monkhorst-Pack grid. Electron-ion interactions are treated with a fully-relativistic pseudopotential approach using the norm-conserving procedure as refined in the optimized norm-conserving Vanderbilt pseudopotential (ONCVPSP) approach [6] with parameters from the Pseudo DOJO library [7] and a cutoff energy on wavefunctions of 80 Ry. Spurious interactions with periodic replicas of the multilayers in the direction orthogonal to the layers are suppressed by using a cutoff on long-range interactions [8]. The band structure is computed over a fine grid using Wannier interpolation [9] and the gap is computed as the energy difference between the bottom of the conduction bands and the top of the valence bands. For each multilayer the energy band gap is computed for several values of the electric field $\mathscr{E}$ by putting charged sheets with uniform and opposite charge densities $\pm\sigma$ at the two sides of the multilayers –thus mimicking a double-gate set up– through the implementation of Ref. [8]. The results of the simulations are discussed in Supplementary Note S8.

DATA AVAILABILITY

The data supporting the findings of this study are available free of charge from the Yareta repository of the University of Geneva, via https://doi.org/10.26037/yareta:txap4ayzibcm5hcipvvzufx72a. This repository contains the data presented in all figures, including those in the Supplementary Information.

[1] Zomer, P. J., Guimarães, M. H. D., Brant, J. C., Tombros, N. & van Wees, B. J. Fast pick up technique for high quality heterostructures of bilayer graphene and hexagonal boron nitride. *Applied Physics Letters* **105**, 013101 (2014).

[2] Domaretskiy, D., Ubrig, N., Gutiérrez-Lezama, I., Tran, M. K. & Morpurgo, A. F. Identifying atomically thin crystals with diffusively reflected light. *2D Materials* **8**, 045016 (2021).

[3] Perdew, J. P., Burke, K. & Ernzerhof, M. Generalized Gradient Approximation Made Simple. *Physical Review Letters* **77**, 3865–3868 (1996).

[4] Giannozzi, P. *et al.* QUANTUM ESPRESSO: a modular and open-source software project for quantum simulations of materials. *Journal of Physics: Condensed Matter* **21**, 395502 (2009).

[5] Giannozzi, P. *et al.* Advanced capabilities for materials modelling with Quantum ESPRESSO. *Journal of Physics: Condensed Matter* **29**, 465901 (2017).

[6] Hamann, D. R. Optimized norm-conserving Vanderbilt pseudopotentials. *Physical Review B* **88**, 085117 (2013).

[7] van Setten, M. J. *et al.* The PseudoDojo: Training and grading a 85 element optimized norm-conserving pseudopotential table. *Computer Physics Communications* **226**, 39–54 (2018).

[8] Sohier, T., Calandra, M. & Mauri, F. Density functional perturbation theory for gated two-dimensional heterostructures: Theoretical developments and application to flexural phonons in graphene. *Physical Review B* **96**, 075448 (2017).

[9] Pizzi, G. *et al.* Wannier90 as a community code: new features and applications. *Journal of Physics: Condensed Matter* **32**, 165902 (2020).